

Cite this: *Green Chem.*, 2012, **14**, 1710

www.rsc.org/greenchem

PAPER

Engineering metal–organic frameworks immobilize gold catalysts for highly efficient one-pot synthesis of propargylamines

Liu Lili,^a Zhang Xin,^{*a,b} Gao Jinsen^a and Xu Chunming^{*a,b}

Received 24th February 2012, Accepted 15th March 2012

DOI: 10.1039/c2gc35284b

Engineering metal–organic frameworks (MOF) for heterogeneous catalysts have been of extreme interest since they could bridge the gap between homogeneous and heterogeneous catalysis. We have designed and synthesized gold functionalized IRMOF-3 catalysts by post-covalent modification (PM) and one-pot (OP) synthesis methods. The gold functionalized IRMOF-3 catalysts provide an efficient, economic, and novel route for the one-pot synthesis of structurally divergent propargylamines *via* three component coupling of alkyne, amine, and aldehyde (A^3) without any additives or an inert atmosphere. The catalysts were characterized in depth to understand their structure–property relationship. It was shown that the 4.6% Au/IRMOF-3 catalyst, prepared by the PM method, contains a fraction of cationic gold ($Au^{3+}/Au^0 = 0.2$), which shows much higher catalytic activity than that of 3.2% or 0.6% Au/IRMOF-3 prepared by OP method, although the former exhibits much lower crystallinity than the latter two catalysts. Notably, the catalytic activity of the Au/IRMOF-3 catalysts could be significantly enhanced at a moderate reaction temperature (150 °C). All the Au/IRMOF-3 catalysts can be easily recycled and used repetitively at least 5 times, especially the catalysts prepared by the OP method, which showed no drop in activity for the successive 5 uses. These features render the catalysts particularly attractive in the practice of propargylamines synthesis in an environmentally friendly manner.

Introduction

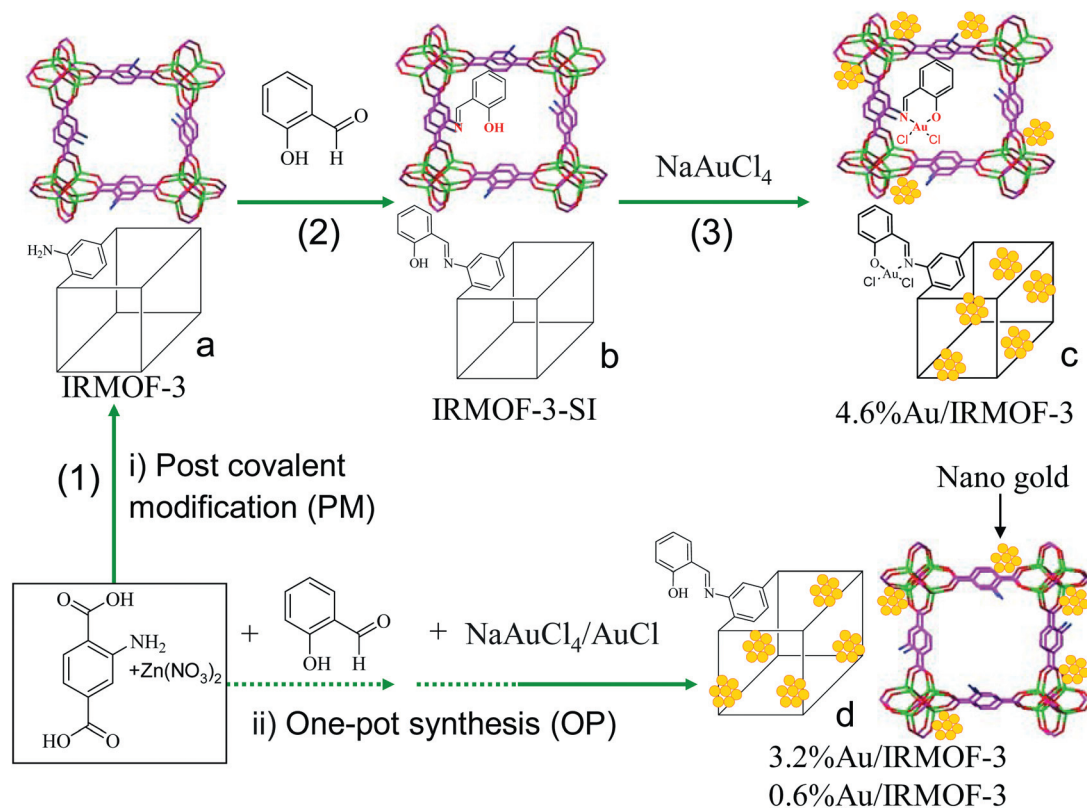
Propargylamines are major skeletons, synthetically versatile and are key intermediates for the preparation of many nitrogen-containing biologically active compounds, such as β -lactams, oxotremorine analogues, conformationally restricted peptides, isosteres, and important structural elements of natural products and therapeutics drug molecules.¹ Conventionally, propargylamines are synthesized by nucleophilic attack of lithium acetylides or Grignard reagents to imines or their derivatives.² However, these methods require the use of stoichiometric amounts of organometallic reagents, strictly controlled reaction conditions, and sensitive functional groups (such as aldehydes) which should be well-protected during the reaction process. An alternative atom-economical approach is to perform this type of reaction by a catalytic coupling of aldehydes, alkynes, and amines (A^3 coupling) by C–H activation, where water is the only theoretical by-product.^{1e,3,4} The significant and pioneering work made by Wei and Li has shown that gold salts ($AuBr_3$ or $AuCl$)

exhibited high activity for the A^3 coupling reaction.⁴ Recent progress in this area has been reported using homogeneous catalysts such as organic gold complexes,⁵ silver salts,⁶ copper salts,⁷ Hg_2Cl_2 ,⁸ and a Cu–Ru^{II} bimetallic system,⁹ among which the cationic gold species showed the highest catalytic activity. However, besides the potential limitations of homogeneous catalysis for achieving a sustainable catalytic process, the rapid reduction of cationic gold species into inactive metallic atoms is unavoidable when gold salts activate alkynes/alkenes.¹⁰

Heterogeneous catalysis offers the opportunity for easy separation and recycling of the catalyst. Thus, the development of improved synthetic methods for the preparation of propargylamines remains an active research area. Remarkably, Kidwai *et al.* reported that a one-pot synthesis of propargylamines can be readily accomplished by using unsupported Au^0 nanoparticles as catalyst.¹¹ The report is indeed significant because the results from the study demonstrate that the Au^0 nanoparticles exhibit excellent alkynophilicity, which is similar to those observed with gold complexes. Recently, Datta *et al.* reported Au nanoparticles, embedded in a mesoporous carbon nitride support with a very low loading of gold function, as an efficient recyclable heterogeneous catalytic system for the one-pot synthesis of propargylamines under atmospheric conditions.¹² Layek *et al.* reported an efficient and highly catalytic system containing Au^0 nanoparticles of the size 10–12 nm that were supported on commercial nano active magnesium oxide plus (NAP–MgO) with ultra low loadings of Au (0.236 mol%) for the one-pot synthesis of

^aState Key Laboratory of Heavy Oil Processing, China University of Petroleum, Beijing 102249, PR China. E-mail: zhangxin@cup.edu.cn; Fax: +86-10-69724721; Tel: +86-10-18911226208

^bThe Key Laboratory of Catalysis, China University of Petroleum, Beijing 102249, PR China. E-mail: xcm@cup.edu.cn; Fax: +86-10-69724721; Tel: +86-10-89733392



Scheme 1 The strategy for gold functionalized IRMOF-3 catalysts by (i) post covalent modification (PM) and (ii) one-pot synthesis (OP).

propargylamines.¹³ Zhang and Corma found that cationic gold species stabilized on CeO₂ and ZrO₂ have much higher catalytic activity in A³ coupling reactions than Au⁰.¹⁴

Metal-organic frameworks (MOFs) are a newly emerging important class of materials, comprising metal “nodes” linked with “rod” shaped organic linkers, which have attracted considerable attention because of their profound range of applications such as in catalysis, separations, and gas storage.¹⁵ Unlike other materials (such as metal oxides), the lack of non-accessible bulk volume and the fully exposed metal sites in MOFs could provide an ultimately high degree of metal dispersion. MOFs supported Au catalysts could help to bridge the gap between homogeneous and heterogeneous Au catalysis for the one-pot synthesis of propargylamines.

The well-known IRMOF-3 consists of Zn₄O clusters linked by 2-amino-1,4-benzenedicarboxylic acid (NH₂-BDC) (Scheme 1a).¹⁶ The high surface area and pore volume observed for IRMOF-3, coupled with uncoordinated amino groups, made it an ideal candidate for devising MOFs with a variety of functionalities.^{17,18} In the present study, IRMOF-3 was functionalized with Au by a post-covalent modification (PM) and one-pot (OP) methods. The functionalized IRMOF-3 catalysts were explored in one-pot synthesis of propargylamines by the A³ coupling reaction of aldehydes, alkynes, and amines. We attempt to establish a relationship between the catalytic performance and catalyst structure, in which the effect of catalyst preparation method, as well as the scope of substrates, recyclability of the catalysts, and the mechanism of A³ coupling reaction were investigated.

Results and discussion

Characterization of catalysts

The IRMOF-3 structure is made of Zn₄O tetranuclear clusters connected by rigid dicarboxylic linkers NH₂-BDC to generate a cubic framework as shown in Fig. 1a and Scheme 1a. The pendant amino groups may serve as a chemical handle that can be manipulated *via* post-synthetic modification with a diverse series of anhydrides, isocyanates and salicylaldehyde.¹⁸ Recently, IRMOF-3 was prepared by different research groups.^{17–19} However, the texture properties of IRMOF-3 were different with each research group. In preliminary work performed by Rowsell *et al.*, IRMOF-3 was solvothermal synthesized with NH₂-BDC and Zn(NO₃)₂·4H₂O in *N,N'*-diethylformamide (DEF) with a BET surface area of 2446 m² g⁻¹.¹⁷ Gascon *et al.* also solvothermal synthesized with a high BET surface area of 3130 m² g⁻¹ in the N₂ protection.^{19b} One of our authors prepared IRMOF-3 with a BET surface area of 750 m² g⁻¹ by a “direct mixing” synthesis strategy at room temperature, following a modification of the procedure described by Huang *et al.*^{18b,20} In the present study, IRMOF-3 was synthesized by a solvothermal method with NH₂-BDC and Zn(NO₃)₂·6H₂O in DMF without N₂ protection. The nitrogen adsorption-desorption isotherms of the solvothermal synthesized IRMOF-3 are displayed in Fig. 1b. The isotherms showed the type IV isotherm with a hysteresis, which indicated this IRMOF-3 material possessed mesoporosity. The mesoporosity should arise from the secondary particle piled pores of the IRMOF-3 crystals. The

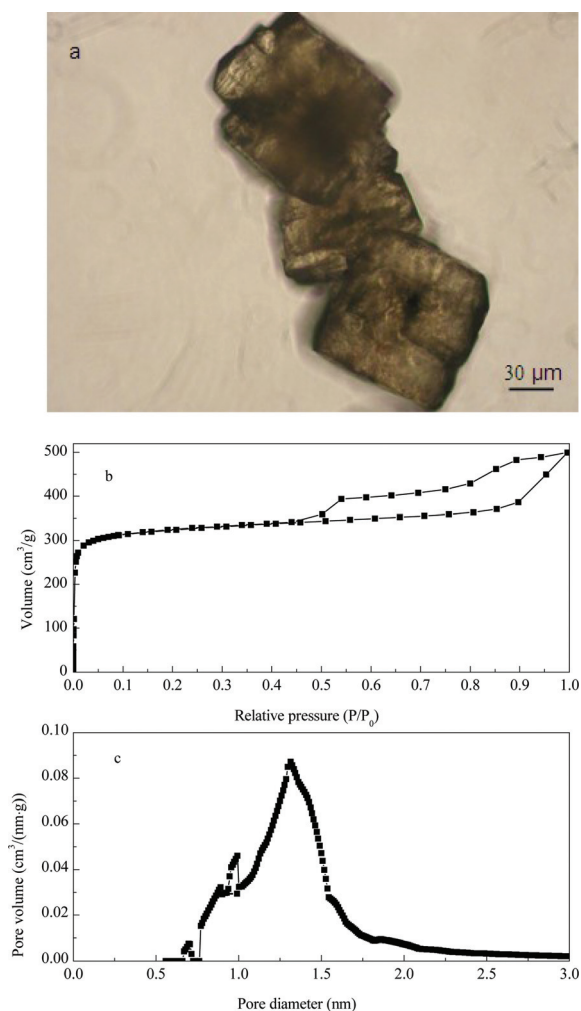


Fig. 1 The optical microscope photograph (a) of IRMOF-3, and N_2 adsorption-desorption isotherms (b), pore size distribution (c).

average pore size of IRMOF-3 was *ca.* 1.3 nm *via* the SF method according to a model of cylinder, as shown in Fig. 1c. The surface area determined by the BET method was $1212 \text{ m}^2 \text{ g}^{-1}$. This value is 62% higher than that ($750 \text{ m}^2 \text{ g}^{-1}$) prepared by the “direct mixing” synthesis,^{18b} but it is still much lower than the $2446 \text{ m}^2 \text{ g}^{-1}$ reported by researchers using DEF as solvent.¹⁷ It was reported that higher BET surface areas could be obtained by using DEF rather than DMF as solvent.^{19b} Moreover, our procedure for preparing IRMOF-3 was not under N_2 protection, although it is well known that MOFs adsorb moisture very quickly upon exposure to ambient air.²¹ Finally, the solvent molecules such as DMF and CHCl_3 could be not completely removed at $50 \text{ }^\circ\text{C}$ before our BET measurement. We have made attempts to improve the BET surface area by changing the degassing conditions, *e.g.*, by degassing at $100\text{--}200 \text{ }^\circ\text{C}$ for 8–12 h or at $50\text{--}60 \text{ }^\circ\text{C}$ for 24–72 h to remove the physically adsorbed DMF, CHCl_3 , and water before BET analysis, however, the BET surface area was not improved. Specifically, when the IRMOF-3 was degassed at *ca.* $200 \text{ }^\circ\text{C}$ for 12 h, the BET surface area even less than $10 \text{ m}^2 \text{ g}^{-1}$, and XRD patterns of the sample indicated that the crystalline structure was decomposed completely.

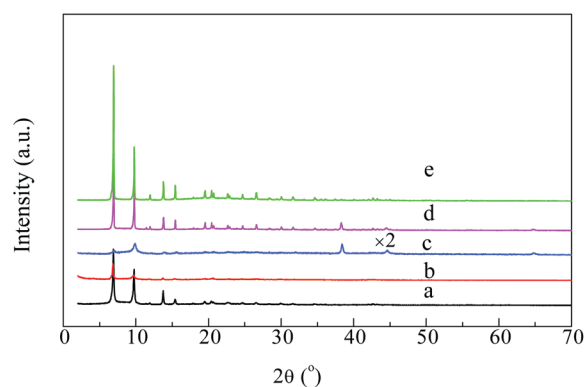


Fig. 2 Powder X-ray diffraction patterns of the different MOFs samples: (a) IRMOF-3, (b) IRMOF-3-SI, (c) 4.6%Au/IRMOF-3, (d) 3.2%Au/IRMOF-3, and (e) 0.6%Au/IRMOF-3.

To prepare the gold functionalized IRMOF-3 catalyst, a strategy including PM (i) and OP (ii) was employed as pictorially shown in Scheme 1. The PM method was followed the procedure as described earlier.^{18b} As can be seen in Scheme 1, it can be comprehended by three steps: (1) IRMOF-3 was firstly synthesized by solvothermal with $\text{NH}_2\text{-BDC}$ and $\text{Zn}(\text{NO}_3)_2 \cdot 6\text{H}_2\text{O}$ in DMF; (2) the IRMOF-3 was then modification with salicylaldehyde to yield IRMOF-3-SI, and salicylideneimine was formed by reaction of the amine of the $\text{NH}_2\text{-BDC}$ ligand with aldehyde group of salicylaldehyde; (3) finally, the NaAuCl_4 was added and 4.6%Au/IRMOF-3 was produced. The detailed describe of each step has been reported earlier.^{18b} The simple and elegant synthesis of gold functionalized IRMOF-3 by OP method is developed as shown in Scheme 1. Typically, a mixture of $\text{NH}_2\text{-BDC}$, $\text{Zn}(\text{NO}_3)_2 \cdot 6\text{H}_2\text{O}$, salicylaldehyde, gold precursor ($\text{AuCl}/\text{NaAuCl}_4$) and DMF with certain ratio of amount was sealed in a teflon-lined stainless steel vessel and heated for 24 h at $100 \text{ }^\circ\text{C}$.

The XRD patterns of IRMOF-3, IRMOF-3-SI, 4.6%Au/IRMOF-3, 0.6%Au/IRMOF-3, and 3.2%Au/IRMOF-3 are shown in Fig. 2. It should be noted that the pattern of IRMOF-3 is very similar to those reported in the literature (Fig. 2a).^{18c,f} Apart from the fact that the intensity of the peak decreases for the IRMOF-3-SI samples, the crystal structure seems to remain unchanged through the post-synthetic modification with salicylaldehyde (Fig. 2b). After IRMOF-3-SI was further functionalized with the solution of NaAuCl_4 , the intensity ratio of typical peaks located at 6.8° and 9.6° became remarkably different from that of IRMOF-3, *i.e.*, the intensity of the peak centered at $2\theta = 6.8^\circ$ for 4.6%Au/IRMOF-3 was severely weakened (Fig. 2c). However, the peak located at $2\theta = 6.8^\circ$ was the strongest one for IRMOF-3. This result could mean that there are some difference for the crystalline structure between 4.6%Au/IRMOF-3 and IRMOF-3. We noted that IRMOF-3 modified by anhydrides with PM method also affected the variance of the intensity ratio for the typical two peaks (see Fig. 4 in ref. 18a, and Fig. 3 in ref. 18b). The change in XRD pattern could be due to the deviation or shrinkage, and even the collapse of pores during the modification process. Wang *et al.* found that a remarkable variation in XRD pattern over Ag/Ni-MOF prepared by the impregnation method compared with Ni-MOF.²² Compared with the sample prepared with PM method, 0.6%Au/IRMOF-3 and 3.2%Au/

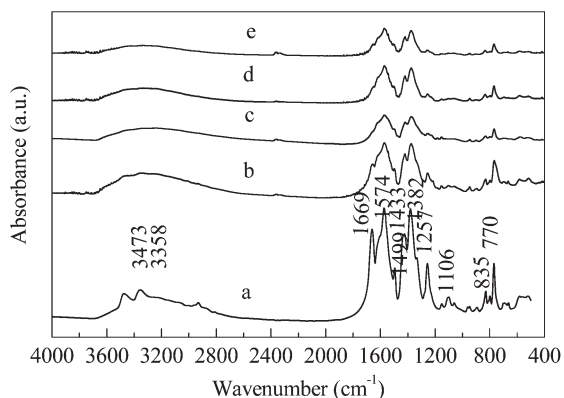


Fig. 3 Infrared spectra of (a) IRMOF-3, (b) IRMOF-3-SI, (c) 4.6% Au/IRMOF-3, (d) 0.6% Au/IRMOF-3, and (e) 3.2% Au/IRMOF-3.

IRMOF-3 prepared by the OP method maintains a higher crystallinity (Fig. 2d and e). It should be pointed out that three additional peaks at $2\theta = 38.2^\circ$, 44.4° , and 64.5° were observed for 4.6% Au/IRMOF-3 and 3.2% Au/IRMOF-3, which were indexed to the (111), (200), and (220) reflection of face centered cubic (fcc) crystalline Au, respectively (JCPDS, card no. 7440-57-5).

Fig. 3 shows the IR spectra of IRMOF-3, IRMOF-3-SI, and gold functionalized IRMOF-3 samples. The IR spectra of IRMOF-3 show two peaks in 3473 and 3358 cm^{-1} due to the existence of the amino groups of the $\text{NH}_2\text{-BDC}$ ligand.²³ However, the N–H stretches at 3473 and 3358 cm^{-1} , associated with the amine of the $\text{NH}_2\text{-BDC}$ ligand, are notably diminished for IRMOF-3-SI and gold functionalized IRMOF-3 samples, which indicated the formation of salicylideneimine by reaction of the amine of the $\text{NH}_2\text{-BDC}$ ligand with the aldehyde group of the salicylaldehyde. For all the samples, the broad bands at 3600–2800 cm^{-1} could be assigned to the stretching vibrations of the O–H in the carboxyl acid and/or phenol groups which originate from $\text{NH}_2\text{-BDC}$ and salicylaldehyde, respectively. The two sharp bands at 1574 and 1382 cm^{-1} corresponds to asymmetric ($\nu_{\text{as}}(\text{C}=\text{O})$) and symmetric ($\nu_{\text{s}}(\text{C}=\text{O})$) vibrations of carboxyl groups, respectively.²⁴ The peaks centered at 1658, 1501, and 1427 cm^{-1} were ascribed to the C=C stretching vibrations of the aromatic. The 1256 cm^{-1} frequency can be assigned to C–N vibrations for all the samples. The bands at ca. 759 cm^{-1} are ascribed to C–H bending vibrations of the monosubstituted benzene.

Fig. 4 shows the TG-DTA curves of IRMOF-3-SI, 4.6% Au/IRMOF-3, 0.6% Au/IRMOF-3, and 3.2% Au/IRMOF-3. The weight loss of these samples could be divided into three stages. The first stage ranged from 50 to 150 $^\circ\text{C}$ was due to the release of physically adsorbed solvent molecules such as CHCl_3 and DMF, which is accompanied with an endothermic peak centered at ca. 100 $^\circ\text{C}$ in the DTA curve. The second stage from 150 to 380 $^\circ\text{C}$ was ascribed to the further release of solvent physically adsorbed within pores or on the surface of the material. The third stage of weight loss over temperatures higher than 380 $^\circ\text{C}$ was due to the decomposition of the crystal structure. The weight loss in the first stage is dramatically influenced by the pretreatment of the sample, and can be higher up to 40% for the

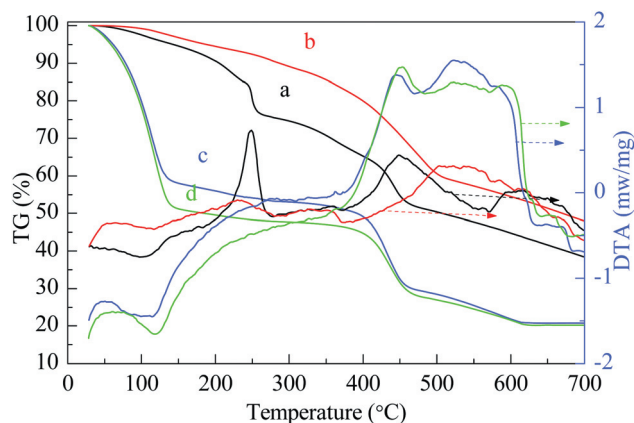


Fig. 4 TG-DTA curves of different samples: (a) IRMOF-3-SI, (b) 4.6% Au/IRMOF-3, (c) 0.6% Au/IRMOF-3, and (d) 3.2% Au/IRMOF-3.

0.6% Au/IRMOF-3 and 3.2% Au/IRMOF-3. Prior to measurement, the samples of 0.6% Au/IRMOF-3 and 3.2% Au/IRMOF-3 were dried in air without further pretreatment. IRMOF-3-SI and 4.6% Au/IRMOF-3 were vacuumed in a rotator at 30–50 $^\circ\text{C}$ for 3–5 h before test. The weight loss of the second stage is dependent on the crystallinity of the samples. The high crystallinity of 0.6% Au/IRMOF-3 and 3.2% Au/IRMOF-3 led to low weight loss (less than 8.0%), while the low crystallinity of IRMOF-3-SI and 4.6% Au/IRMOF-3 led to a much higher weight loss (up to 27.4%). This result indicates that the samples prepared *via* the one-pot synthesis have higher thermal stabilities compared with the samples prepared by the post-covalent modification. For all the samples, a significant exothermic peak can be observed in their DTA curves for the sharp weight loss of the third stage. TG-DTA experiments showed that 4.6% Au/IRMOF-3, 0.6% Au/IRMOF-3, and 3.2% Au/IRMOF-3 decompose when the temperature is higher than ca. 380 $^\circ\text{C}$, which showed lower thermal stabilities than IRMOF-3 with a decomposition temperature of ca. 430 $^\circ\text{C}$.^{18a,d}

TEM measurements were conducted to analyze the size and morphology of the Au in 4.6% Au/IRMOF-3, 0.6% Au/IRMOF-3, and 3.2% Au/IRMOF-3. Fig. 5 shows the representative TEM images and particle size distribution. It was shown that the Au nanoparticles were close to spherical with average diameters of 3.3, 1.7, and 2.5 nm for 4.6% Au/IRMOF-3, 0.6% Au/IRMOF-3, and 3.2% Au/IRMOF-3, respectively. After four successive cycles, the Au nanoparticles of 4.6% Au/IRMOF-3 appeared significantly agglomerated with maximum sizes up to 34.5 nm, while the average size increased to 13.8 nm (Fig. 5d). The Au nanoparticles of 3.2% Au/IRMOF-3 also appeared agglomerated after four successive cycles, and the average size of Au nanoparticles was increased from 2.5 to 12.0 nm (Fig. 5e). We anticipated the preparation of a MOF containing a Au(III) Schiff base complex lining the pore wall. However, the agglomeration of the Au nanoparticles is clear, as depicted from TEM analysis (Fig. 5). Nevertheless, we cannot rule out the possibility of cationic gold species existing on functionalized IRMOF-3, since the cationic gold species cannot be detected by TEM and the exposure to electron beams under high vacuum during TEM measurements might also effect changes in the gold oxidation state.²⁵

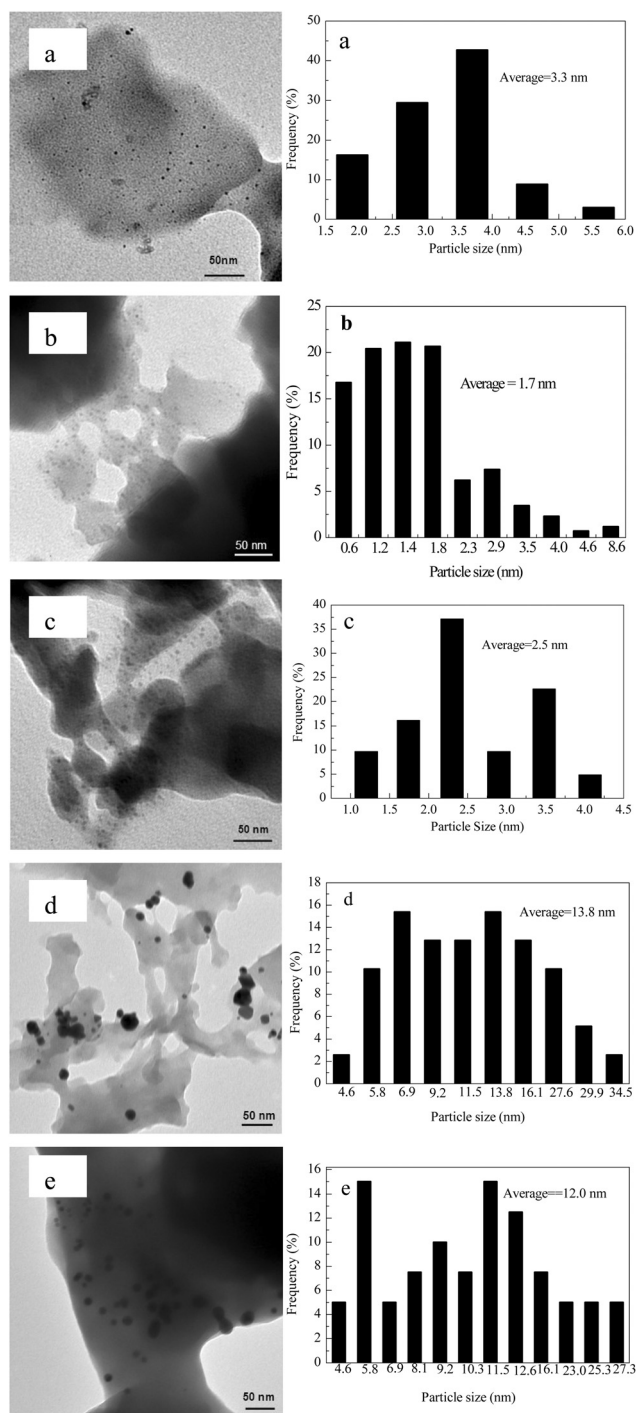


Fig. 5 TEM images and particle size distribution of (a) 4.6% Au/IRMOF-3, (b) 0.6% Au/IRMOF-3, (c) 3.2% Au/IRMOF-3, (d) 4.6% Au/IRMOF-3 after four runs, and (e) 3.2% Au/IRMOF-3 after four runs.

We have made an attempt to characterize the gold oxidation states of 4.6% Au/IRMOF-3 and 3.2% Au/IRMOF-3 by XPS. However, the overlap of binding energies between Au 4f and Zn 3p made it very difficult to discern the exact binding energy of Au 4f. Moreover, it is understood that quantitative assessment of the gold oxidation state by XPS characterization is limited because the final state effects associated with particle size could

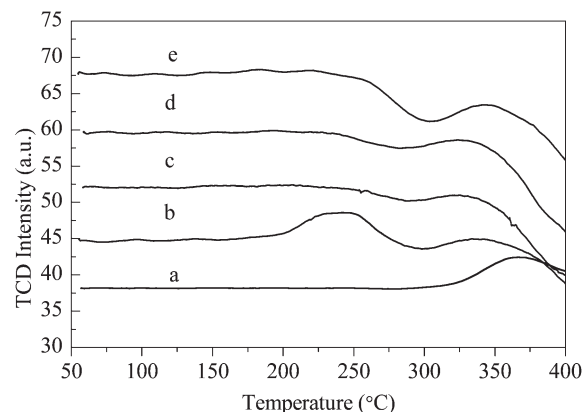


Fig. 6 TPR profiles of (a) IRMOF-3-SI, (b) 4.6% Au/IRMOF-3, (c) 0.6% Au/IRMOF-3, (d) 3.2% Au/IRMOF-3, and (e) 4.6% Au/IRMOF-3 after four successive cycles.

heavily disturb the XPS features of Au and the exposure to photoelectrons under high vacuum during XPS measurements, which might also effect changes in the gold oxidation state.^{25c} Excellent work by Wang *et al.* has shown that the oxidation states of silver supported on Ni-MOF could be discerned using UV-vis spectrometry and cyclic voltametry,²² by which, however, it is still difficult to quantitatively measure the exact amount of gold species with a mixture of metallic and cationic ions.

The TPR technique is usually used to quantitatively measure the reduction of oxidized gold species and thereby calculate the distribution of different gold oxidation states in supported Au catalysts.^{18f,26} Fig. 6 shows H₂-TPR profiles of IRMOF-3-SI, 4.6% Au/IRMOF-3, 0.6% Au/IRMOF-3, and 3.2% Au/IRMOF-3. IRMOF-3-SI exhibits only one peak in the range of 300–400 °C. The TPR profile of 4.6% Au/IRMOF-3 features two hydrogen consumption peaks, one is located at a relatively low temperature range (190–270 °C) and another is located at temperatures higher than 300 °C, while only one peak, located at higher temperatures, was found for 0.6% Au/IRMOF-3 and 3.2% Au/IRMOF-3. There was also no H₂-consumption peak at low temperatures (190–270 °C) for the catalyst of 4.6% Au/IRMOF-3 after four successive cycles. One of our authors has previously observed two reduction peaks over IRMOF-3-SI-Au, while only one reduction peak located at a high temperature range was found on IRMOF-3-SI.^{18b} Similar to the previous work, we presume that the low temperature peak was due to the reduction of Au³⁺ ions into Au⁰ atoms, and the ratio of Au³⁺/Au⁰ for 4.6% Au/IRMOF-3 is 0.2. The higher temperature peak was ascribed to the decomposition of the support of IRMOF-3. The catalyst model can be illustrated as in Scheme 1. It should be pointed out that a mixture of Au⁰ and Au³⁺ was obtained by using the post-covalent modification, however, only cationic Au³⁺ species were found in the earlier report.^{18b} No peak that was characteristic of Au³⁺ reduction was found on 0.6% Au/IRMOF-3 and 3.2% Au/IRMOF-3 samples which were prepared by OP method at 100 °C for 24 h, as well as for the 4.6% Au/IRMOF-3 after four successive cycles. We presume that the cationic gold species could be reduced into metallic gold atoms during the synthesis. It has been reported that cationic gold species are easily reduced,

even at room temperature, and that alkynes, alkenes, alcohols, CO, and phosphines present in the reaction media are the reducing agents.²⁷

We suggest that the above results of the characterizations with IRMOF-3 immobilized gold catalysts can be understood on the basis of models as depicted in Scheme 1. For 4.6%Au/IRMOF-3 prepared by PM method, the active catalyst contains both metallic gold nanoparticles and cationic Au³⁺ ions (Scheme 1c). Since the average diameter of gold nanoparticles on the 4.6%Au/IRMOF-3 catalyst is 3.3 nm, which is clearly much larger than that of the average pore size of IRMOF-3 (1.3 nm), the gold nanoparticles should be deposited on the surface of IRMOF-3 as shown in Scheme 1c. The Au³⁺ ions are coordinated by O, N and Cl atoms and are present as a Schiff base complex.^{18b} In the cases of the 3.2%Au/IRMOF-3 and 0.6%Au/IRMOF-3 catalysts prepared by the OP method, only metallic gold nanoparticles were verified by the H₂-TPR analysis. Due to their larger diameters (2.5, 1.7 nm) of gold nanoparticles compared with the average pore size of IRMOF-3, the gold nanoparticles should be also deposited on the surface of IRMOF-3 (Scheme 1d). The structures of Au/IRMOF-3 catalysts are not, however, fixed: (i) the gold nanoparticles are clearly aggregated during the A³ coupling reaction, (ii) the cationic Au³⁺ ions on the 4.6%Au/IRMOF-3 catalyst may change during the A³ coupling reaction and were found to be completely reduced into metallic gold atoms after four successive cycles.

Catalytic studies

Fig. 7 shows the kinetic curves for 4.6%Au/IRMOF-3, 0.6%Au/IRMOF-3, and 3.2%Au/IRMOF-3 for the A³ coupling reaction of benzaldehyde, phenylacetylene, and piperidine with 1,4-dioxane as solvent at 120 °C. It can be seen that 3.2%Au/IRMOF-3 has a higher conversion of benzaldehyde than 0.6%Au/IRMOF-3. Maximum conversions of 8.0% and 16.0% were obtained within 5 h over 0.6%Au/IRMOF-3 and 3.2%Au/IRMOF-3, respectively. However, the conversion reached 77.0% in 0.5 h over 4.6%Au/IRMOF-3 at 120 °C, and then remained constant. Taking into account the total Au content of the catalyst,

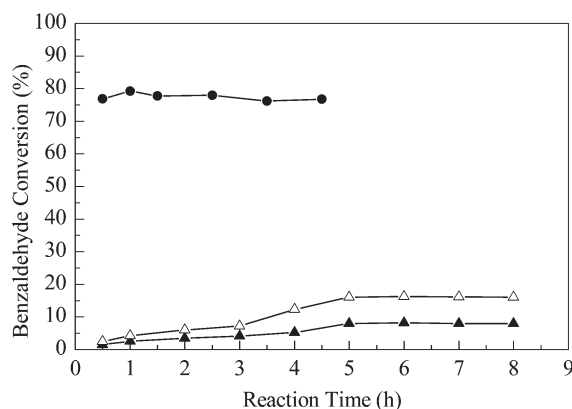


Fig. 7 Comparison of the catalytic activity over 4.6%Au/IRMOF-3 (●), 0.6%Au/IRMOF-3 (▲), and 3.2%Au/IRMOF-3 (△) for A³ coupling reaction of benzaldehyde (0.25 mmol), phenylacetylene (0.33 mmol), and piperidine (0.30 mmol) with 1,4-dioxane (1.0 mL) as solvent at 120 °C.

the reaction rates from the maximum conversions were calculated to be 120.5, 9.2, and 3.6 mmol g_{Au}⁻¹ h⁻¹ for 4.6%Au/IRMOF-3, 0.6%Au/IRMOF-3, and 3.2%Au/IRMOF-3, respectively, and the TON numbers calculated were 12, 9, and 4, respectively. It is evident that the reaction rate of 4.6%Au/IRMOF-3 is one order of magnitude higher than those of 0.6%Au/IRMOF-3 and 3.2%Au/IRMOF-3. We noted that the benzaldehyde conversions over 0.6%Au/IRMOF-3 and 3.2%Au/IRMOF-3 can be remarkably enhanced by increasing the reaction temperature from 120 to 150 °C. As shown in Fig. 8, the conversions were continuously increased to *ca.* 98% within 12 h on both catalysts. The reaction rates calculated on the basis of total gold weight at 150 °C are 47.3 and 10.9 mmol g_{Au}⁻¹ h⁻¹ for 0.6%Au/IRMOF-3 and 3.2%Au/IRMOF-3, respectively, and the TON numbers are 112 and 22, respectively.

To examine the scope of the A³ coupling reaction, we extended our studies to different combinations of aldehydes, amines, and alkynes. The results are summarized in Table 1. Aromatic aldehydes including those bearing functional groups such as alkoxy, alkyl, and chloro were able to undergo the corresponding three-component-coupling, and afforded good conversions of aldehydes in the A³ coupling reaction (Table 1, entries 1–6, 15–24). It was found that aryl aldehydes possessing electron-withdrawing groups (Table 1, entry 4) afforded a higher conversion than those with an electron-donating group bound to the benzene ring (Table 1, entries 2 and 3) over 4.6%Au/IRMOF-3 catalyst. However, aryl aldehydes with electron-donating groups gave higher conversions than aryl aldehydes with electron-withdrawing groups for the 0.6%Au/IRMOF-3 (Table 1, entry 16 vs. 17) and 3.2%Au/IRMOF-3 (Table 1, entry 21 vs. 22) catalysts. Notably, aliphatic aldehydes such as cyclohexanecarboxaldehyde and *n*-octaldehyde display higher activities than aromatic aldehydes with the 4.6%Au/IRMOF-3, 0.6%Au/IRMOF-3, and 3.2%Au/IRMOF-3 (Table 1, entries 5, 6, 18, 19, 23, 24). While unwanted trimerization of aliphatic aldehydes is a major limitation of the A³ coupling reactions catalyzed by homogeneous catalysts,^{5,9,28} no trimer could be detected with the supported Au catalyst. A referee of the present paper noticed that the activity difference between 4.6%Au/IRMOF-3 and 0.6%Au/IRMOF-3, 3.2%Au/IRMOF-3 catalysts, *i.e.*, aromatic aldehydes

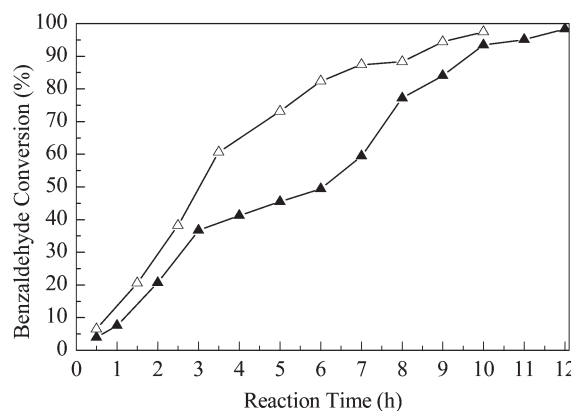


Fig. 8 Comparison of the catalytic activity over 0.6%Au/IRMOF-3 (▲) and 3.2%Au/IRMOF-3 (△) for A³ coupling reaction of benzaldehyde (0.25 mmol), phenylacetylene (0.33 mmol), and piperidine (0.30 mmol) with 1,4-dioxane (1.0 mL) as solvent at 150 °C.

Table 1 Coupling of aldehyde, alkyne, and amine catalyzed by Au/IRMOF-3 in 1,4-dioxane^a

$$\text{R}^1\text{-CHO} + \text{R}^2\text{R}^3\text{NH} + \text{R}^4\text{-C}\equiv\text{C-H} \xrightarrow[\text{Au/IRMOF-3}]{\text{dioxane } 120/150^\circ\text{C}} \text{R}^1\text{-C}(\text{NR}^2\text{R}^3)\text{-C}\equiv\text{C-R}^4$$

Entry	Cat.	R ¹	R ² R ³ NH	R ⁴	T ^b (h)	Conv./Yield ^c (%)
1	4.6%Au/IRMOF-3	Ph	Piperidine	Ph	0.5	77.0
2	4.6%Au/IRMOF-3	4-MeC ₆ H ₄	Piperidine	Ph	12	70.6
3	4.6%Au/IRMOF-3	4-MeOC ₆ H ₄	Piperidine	Ph	12	38.6
4	4.6%Au/IRMOF-3	3-ClC ₆ H ₄	Piperidine	Ph	12	95.4
5	4.6%Au/IRMOF-3	Cyclohexyl	Piperidine	Ph	12	98.9
6	4.6%Au/IRMOF-3	Heptyl	Piperidine	Ph	12	96.3
7	4.6%Au/IRMOF-3	Ph	Pyrrolidine	Ph	12	91.2
8	4.6%Au/IRMOF-3	Ph	Morpholine	Ph	12	54.6
9	4.6%Au/IRMOF-3	Ph	Diethylamine	Ph	12	26.6
10	4.6%Au/IRMOF-3	Ph	Piperidine	4-MeC ₆ H ₄	12	86.4
11	4.6%Au/IRMOF-3	Ph	Piperidine	4-EtC ₆ H ₄	12	70.6
12	4.6%Au/IRMOF-3	Ph	Piperidine	4-ButC ₆ H ₄	12	28.5
13	4.6%Au/IRMOF-3	Ph	Piperidine	Hexyl	12	62.1
14	4.6%Au/IRMOF-3	Ph	Piperidine	(CH ₃) ₃ Si	12	56.6
15	0.6%Au/IRMOF-3	Ph	Piperidine	Ph	12	98.0
16	0.6%Au/IRMOF-3	4-MeC ₆ H ₄	Piperidine	Ph	24	75.0
17	0.6%Au/IRMOF-3	3-ClC ₆ H ₄	Piperidine	Ph	24	40.3
18	0.6%Au/IRMOF-3	Cyclohexyl	Piperidine	Ph	24	98.2
19	0.6%Au/IRMOF-3	Heptyl	Piperidine	Ph	24	97.6
20	3.2%Au/IRMOF-3	Ph	Piperidine	Ph	10	98.0
21	3.2%Au/IRMOF-3	4-MeC ₆ H ₄	Piperidine	Ph	24	65.2
22	3.2%Au/IRMOF-3	3-ClC ₆ H ₄	Piperidine	Ph	24	30.0
23	3.2%Au/IRMOF-3	Cyclohexyl	Piperidine	Ph	24	98.5
24	3.2%Au/IRMOF-3	Heptyl	Piperidine	Ph	24	96.8

^a Reaction conditions: aldehyde (0.250 mmol), amine (0.300 mmol), alkyne (0.325 mmol), catalyst (0.07 g), the reaction temperatures are 120, 150, and 150 °C on 4.6%Au/IRMOF-3, 0.6%Au/IRMOF-3, and 3.2%Au/IRMOF-3 catalysts, respectively. ^b The reaction time was not optimization. ^c GC yield or conversion based on aldehydes, the product was determined by GC-MS, and ¹H-NMR.

bearing electron-withdrawing groups (Table 1, entry 4) afforded a better yield than those bearing electron-donating groups (Table 1, entries 2 and 3) when 4.6%Au/IRMOF-3 catalyst was used, however, the employment of 0.6%Au/IRMOF-3 (Table 1, entry 17 vs. 16) and 3.2%Au/IRMOF-3 (Table 1, entry 22 vs. 21) gave the opposite results. The A³ coupling reaction was reported to be highly affected by the nature of aldehydes, and the reactivity of aldehydes could be affected by the employed catalyst.^{4,6,14,22,29} Kidwai *et al.* found that aryl aldehydes possessing electron-withdrawing groups afforded a better yield than that with an electron-donating group bound to the benzene ring which required longer reaction time with metallic Au nanoparticles as catalyst.¹¹ Wei and Li reported that both aromatic and aliphatic aldehydes were able to undergo the corresponding A³ coupling with the catalyst of AuBr₃.⁴ They found that electron-withdrawing groups displayed high reactivities, however, electron-rich groups bound to the benzene ring decreased the reactivity and required a longer reaction time. The decreased yield for aliphatic aldehydes was caused by the trimerization of aliphatic aldehydes with homogeneous gold salts. Zhang and Corma found that benzaldehyde with electron-donating groups react smoothly, while substitution of electron-withdrawing groups on the benzene ring decreases the reactivity with the catalyst of Au/CeO₂.¹⁴ Based on the above results, we may presume that the activity difference could be due to the different properties (*e.g.*, different oxidation states) between 4.6%Au/IRMOF-3 and 0.6%Au/IRMOF-3, 3.2%Au/IRMOF-3 catalysts.

With the catalyst of 4.6%Au/IRMOF-3, the reaction with secondary amines proceeded smoothly to afford the corresponding propargylamines (Table 1, entries 1, 7–9). Among the various amines tested, alicyclic amines such as piperidine, pyrrolidine, and morpholine gave good conversions of benzaldehyde, whereas the diethylamine afforded a lower conversion. This was probably due to the iminium ions generated from alicyclic amines and benzaldehyde which are more stable than that generated from dialkyl amine and benzaldehyde.

A variety of aromatic alkynes were coupled with benzaldehyde and piperidine in the presence of the 4.6%Au/IRMOF-3 catalyst. It was found that straight-chain alkyl substituted phenylacetylene showed decreasing conversion of benzaldehyde with increasing chain length, the conversions were 86.4%, 70.6%, and 28.5% for methyl, ethyl, and butyl phenylacetylene, respectively (Table 1, entries 10–12). Clearly, when increasing the steric hindrance of alkynes, it gave a decrease in conversion. The reaction was found to be highly affected by the steric hindrance of the alkynes, which was probably ascribed to the limitation effect of the IRMOF-3 channels. Aliphatic alkynes such as 1-octyne and (trimethylsilyl)acetylene also afforded moderate conversions of benzaldehyde with 62.1% and 56.6%, respectively (Table 1, entries 13 and 14).

The reusability studies of 4.6%Au/IRMOF-3, 0.6%Au/IRMOF-3, and 3.2%Au/IRMOF-3 were carried out on the A³ coupling reaction of benzaldehyde, piperidine, and phenylacetylene. The results are summarized in Table 2. The fresh 4.6%Au/

IRMOF-3 gave a benzaldehyde conversion of 77% within 0.5 h. After four successive cycles with intermediate extensive washing with 1,4-dioxane, the conversions over 4.6%Au/IRMOF-3 were 75%, 73%, 62%, and 66% at reaction times of 5, 12, 12 and 13 h, respectively. Clearly, 4.6%Au/IRMOF-3 features a slight deactivation mode. However, no drop in activity was found over 0.6%Au/IRMOF-3 and 3.2%Au/IRMOF-3 which were prepared by the one-pot synthesis. Specifically, the conversions over 3.2% Au/IRMOF-3 for the fresh and three successive cycles are 97%, 98%, 98%, and 97% at reaction time of 10, 7, 9, and 10 h, respectively. The fourth reuse of 0.6%Au/IRMOF-3 showed a slight decrease in the conversion. Considering that the sizes of the gold nanoparticles for the recycled 4.6%Au/IRMOF-3 and 3.2%Au/IRMOF-3 catalysts were aggregated from 3.3, 2.5 nm to 13.8, 12.0 nm, respectively (Fig. 5), we can rule out the possibility that the deactivation mode of 4.6%Au/IRMOF-3 is due to the conglomeration of Au nanoparticles. This conclusion agrees very well with the work of Kidwai *et al.*, who found that unsupported gold nanoparticles with average sizes of 10, 20, or 30 nm gave very similar benzaldehyde conversions (*ca.* 90%).¹¹ As it was well established that cationic gold species showed higher catalytic activity than that of metallic gold counterpart for the A³ coupling reaction,^{4,14} the deactivation of 4.6%Au/IRMOF-3 could be due to the reduction of Au³⁺ as demonstrated by the TPR analysis (Fig. 6). It should be pointed out that there is a slight leaching of gold (*ca.* 5%) over the recycled 4.6%Au/IRMOF-3, however, there is no leaching of gold over the recycled 3.2%Au/IRMOF-3 and 0.6%Au/IRMOF-3 catalysts evidenced by ICP-AES analysis. The slight leaching of gold could also be responsible for the deactivation of 4.6%Au/

IRMOF-3. We presume that the high crystallinity and thermal stability of the 3.2%Au/IRMOF-3 and 0.6%Au/IRMOF-3 catalysts provide the advantage of resisting gold leaching.

Wei and Li have initially reported the A³ coupling catalyzed using homogeneous gold catalysts (*e.g.*, AuBr₃),⁴ while silver, copper, and mercury salts were also found to be able to catalyze the reaction.^{6–8} However, as mentioned earlier, the limitations and the deactivation for homogeneous catalysts make it impossible for sustainable catalytic processes. By investigating several heterogeneous gold catalysts for the A³ coupling reaction, using benzaldehyde, phenylacetylene and piperidine as a model reaction, we could evaluate their catalytic performance as summarized in Table 3. Unsupported Au nanoparticles (*ca.* 20 nm) showed good catalytic activity, *i.e.*, 97% conversion of benzaldehyde in 5 h at 75–80 °C.¹¹ The reaction rate and TON based on total Au contents were only *ca.* 9.8 mmol g_{Au}⁻¹ h⁻¹ and 9, respectively. Gold on layered double hydroxide (LDH–AuCl₄) afforded the desired propargylamines with a reaction rate and TON of *ca.* 31.0 mmol g_{Au}⁻¹ h⁻¹ and 30, respectively, in refluxing THF (*ca.* 80 °C).³⁰ However, the activity of the catalysts sharply decreased in the successive reuse (92% yield of the fresh to 40% in the second use). The reaction rate of Au nanoparticles (*ca.* 7 nm) encapsulated over mesoporous carbon nitride afforded a 96% yield at 100 °C in 24 h, whereas the catalytic efficiency has only been demonstrated for very few substrates and its reuse has not been reported.¹² Layek *et al.* reported that Au⁰ nanoparticles (10–12 nm) supported on commercial nano active magnesium oxide plus showed high yields of 96% in 24 h at 100 °C with a reaction rate and TON of 436.7 mmol g_{Au}⁻¹ h⁻¹ and 407, respectively.¹³ CeO₂ supported gold nanoparticles (2–5 nm) gave benzaldehyde conversion up to 99% in 6 h at 100 °C with a TON as high as 788, however, the leaching of gold was unavoidable for the first reuse.¹⁴ Based on the above results, our 4.6%Au/IRMOF-3 catalyst shows much higher reaction rates (120.5 mmol g_{Au}⁻¹ h⁻¹) than unsupported gold nanoparticles and LDH–AuCl₄. Although its TON number is little smaller than LDH–AuCl₄, the catalyst shows good stability and can be reused at least 4 times. The 0.6%Au/IRMOF-3 and 3.2%Au/IRMOF-3 catalysts prepared by the one-pot synthesis method showed improved catalytic activity at a moderate reaction temperature (150 °C). Specifically, the 0.6%Au/IRMOF-3 shows a reaction rate of 47.3 mmol g_{Au}⁻¹ h⁻¹ and TON number of 112. Although the activity is still less than those of NAP–MgO and Au/CeO₂, the excellent performance of the catalyst reuse shows the advantage of using the IRMOF-3 as a stabilizer.

Table 2 Recyclability of Au/IRMOF-3 in A³ coupling reaction of benzaldehyde, piperidine, and phenylacetylene^a

Run	4.6%Au/IRMOF-3 ^b		0.6%Au/IRMOF-3 ^c		3.2%Au/IRMOF-3 ^c	
	Time (h)	Conv. (%)	Time (h)	Conv. (%)	Time (h)	Conv. (%)
Fresh	0.5	77	12	98	10	97
1	5	75	7	98	7	98
2	12	73	7	94	9	98
3	12	62	8	93	10	97
4	13	66	9	90		

^a Reaction conditions: benzaldehyde (0.250 mmol), piperidine (0.300 mmol), phenylacetylene (0.325 mmol), and 1,4-dioxane (1.0 g), catalyst (0.07 g). ^b 120 °C. ^c 150 °C.

Table 3 The reaction rate and TON with different heterogeneous gold catalysts in A³ coupling reaction

Catalyst	Average size of Au (nm)	Au oxidation states	Time (h)	Conv./Yield (%)	Reaction rate (mmol g _{Au} ⁻¹ h ⁻¹)	TON	Ref.
4.6%Au/IRMOF-3	3.3	Au ³⁺ , Au ⁰	0.5	77	120.5	12	This work
0.6%Au/IRMOF-3	1.7	Au ⁰	12	98	47.3	112	This work
3.2%Au/IRMOF-3	2.5	Au ⁰	10	97	10.9	22	This work
Unsupported Au nanoparticles	20	Au ⁰	5	97	9.8	9	11
LDH–AuCl ₄	—	Au ³⁺	5	92	31.0	30	30
Au–MCN	7	Au ⁰	24	96	—	—	12
NAP–MgO	10–12	Au ⁰	24	96	436.7	407	13
Au/CeO ₂	2–5	Au ³⁺ , Au ⁰	6	99	659.5	788	14

Taking into account our reaction results and the previous reports, we may infer that the A^3 coupling reaction is insensitive for the size of gold nanoparticles. One evidence comes from the fact that high catalytic activity could be obtained on various sizes of gold nanoparticles (1.7–50.0 nm).^{11–14} Another evidence may lie in the fact that the activity is not changed for the three successive reused 0.6%Au/IRMOF-3 and 3.2%Au/IRMOF-3 catalysts, although their sizes of gold nanoparticles significantly aggregated (Fig. 5). Finally, Kidwai *et al.* found that unsupported gold nanoparticles with average sizes of 10, 20, 30, and 50 nm exhibited very similar yields (73%–92%), although the gold nanoparticles with *ca.* 20 nm showed a little higher reaction rates.¹¹

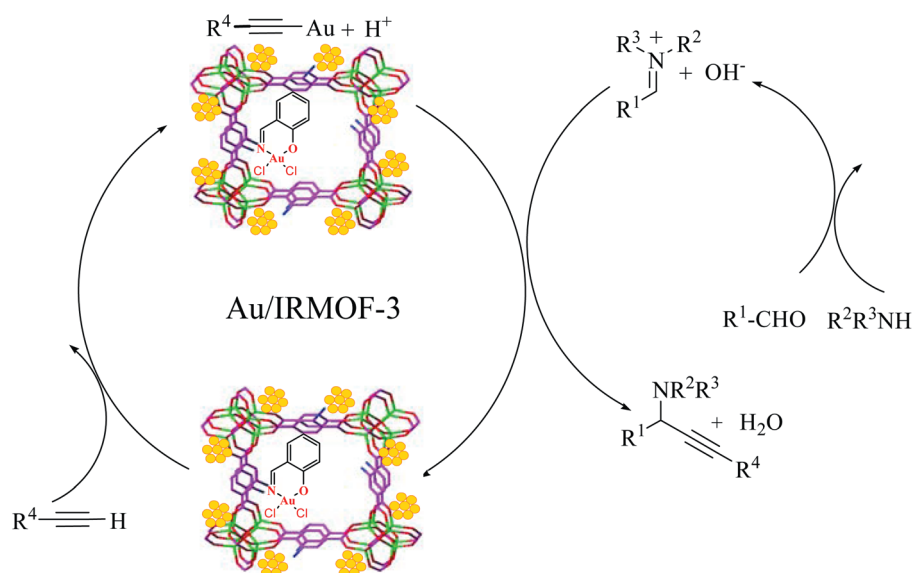
Based on the above discussion, and taking views that the size of gold nanoparticles is insensitive for the A^3 coupling reaction, we presume that the higher reaction rate and TON number of 4.6%Au/IRMOF-3 than 0.6%Au/IRMOF-3 and 3.2%Au/IRMOF-3 at 120 °C were most probably due to the effect of gold oxidation states. The appearance of Au^{3+} ions on 4.6%Au/IRMOF-3, while only metallic gold on the latter two catalysts as demonstrated by TPR was the prominent difference on the three catalysts. Wei and Li found that metallic gold sponge showed not any activity for the A^3 coupling reaction at 100 °C.⁴ Kantam *et al.* found that the activity of LDH– $AuCl_4$ sharply decreased with the reduction of Au^{3+} ions into Au^+ and Au^0 .³⁰ Zhang and Corma also found that the catalytic activity of Au^{3+} supported on nanocrystalline ZrO_2 and CeO_2 is much higher than Au^0 in A^3 coupling reaction.¹⁴ Therefore a fraction of cationic Au^{3+} ($Au^{3+}/Au^0 = 0.2$) in the 4.6%Au/IRMOF-3 catalyst should be responsible to the higher catalytic activity than those of 0.6%Au/IRMOF-3 and 3.2%Au/IRMOF-3 with only metallic gold counterpart.

We speculate that the reaction mechanism of these supported Au catalysts (Scheme 2) could be the same as that with cationic gold and/or Au^0 .^{4,11,14} A tentative mechanism was proposed involving the absorption of alkyne followed by the insertion of Au^{3+} and/or Au^0 nanoparticles stabilized by the metal–organic

frameworks into the C–H bond. The alkenyl–Au intermediate then reacted with the iminium ion generated *in situ* from the aldehydes and secondary amines to give the corresponding propargylamines and to regenerate the Au^{3+} and/or Au^0 nanoparticles catalysts for further reactions.

Conclusions

In conclusion, we have shown that gold functionalized IRMOF-3 catalysts can be achieved by using the strategies of post-covalent modification and one-pot synthesis. The 4.6%Au/IRMOF-3 catalyst prepared by the PM method contains gold nanoparticles with an average size of 3.3 nm and features a mixture of Au^0 and Au^{3+} . The 0.6%Au/IRMOF-3 and 3.2%Au/IRMOF-3 catalysts prepared by the OP method show higher crystallinity and contain metallic gold nanoparticles with average sizes of 1.7, and 2.5 nm, respectively. These catalysts were explored in A^3 coupling reactions of aldehydes, amines, and alkynes, and showed good to excellent conversions of aldehydes and 100% selectivity for propargylamines. It was also shown that the catalytic activity of 4.6%Au/IRMOF-3 was higher than 0.6%Au/IRMOF-3 and 3.2%Au/IRMOF-3 at 120 °C. The reaction rate and TON can be greatly enhanced by increasing the reaction temperature of 150 °C for 0.6%Au/IRMOF-3 and 3.2% Au/IRMOF-3 catalysts. The appearance of cationic Au^{3+} on 4.6%Au/IRMOF-3 is the main reason for the higher catalytic activity. The size of the gold nanoparticles is insensitive for the catalytic activity of A^3 coupling reaction. The A^3 coupling reaction catalyzed by IRMOF-3 immobilized gold catalysts renders broad substrate applicability. And the catalysts can readily be recovered and reused for at least 4 cycles. No loss of activity was found for the 0.6%Au/IRMOF-3 and 3.2%Au/IRMOF-3 catalysts with higher crystallinity and thermal stability as compared with 4.6%Au/IRMOF-3. These features render the catalysts particularly attractive in the practice of propargylamines synthesis in an environmentally friendly manner.



Scheme 2 Probable mechanism of the A^3 -coupling catalyzed by Au/IRMOF-3.

Experimental

Materials and methods

All the chemicals purchased are of reagent grade and were used without further purification. The crystal structures of the samples were characterized by powder X-ray diffraction (XRD) on a Brüker D8 Advance diffractometer at 40 kV and 40 mA for Cu K α , with a scan speed of 10° min⁻¹ and a step size of 0.02° in 2 θ . Surface areas of the samples were measured with nitrogen adsorption at 77 K on a Quantachrome instrument. For each measurement, the sample was degassed at 50 °C for 13 h to remove any loosely held adsorbed species, then analyzed at 77 K with N₂ analysis gas. The surface area and pore volume were determined by the Brunauer–Emmett–Teller (BET) method, and the average pore size was calculated from the desorption branch by using the Staito–Foley (SF) method. Thermogravimetric analysis (TGA) and differential thermal (DTA) analyses were measured in a Mettler Toledo TGA/SDTA 851 instrument in flowing nitrogen (50 mL min⁻¹) with a rate of 10 °C min⁻¹. The samples of IRMOF-3-SI and 4.6%Au/IRMOF-3 were vacuumed in a rotator at 30–50 °C for 3–5 h before test. The TG-DTA curves were obtained with the as-synthesized 0.6%Au/IRMOF-3 and 3.2%Au/IRMOF-3 drying in air without further pretreatment. Infrared (IR) spectra (400–4000 cm⁻¹) were recorded from KBr pellets in a 2000FT-IR spectrometer. The metal (Au) contents were determined by inductively coupled plasma (ICP) on an Optima 7000 DV instrument. Transmission electron microscopy (TEM) was used to determine the Au particle size distribution and morphology of the samples. The specimens were prepared by grinding with a mortar and the resulting powder was then sonicated in ethanol to achieve good dispersion. The solution was dropped onto a holey carbon coated 300 mesh copper grid (SPI). The samples were dried and then analyzed with JSM-200CX transmission electron microscope. X-Ray photoelectron spectroscopy (XPS) measurements were carried out in an ARL-9800 instrument. The temperature-programmed-reduction (TPR) measurement was conducted on a home-made apparatus equipped with a TCD detector. The catalysts were pretreated at 50 °C for 0.5 h under argon. The catalysts were subsequently contacted with a 6.0%H₂/Ar mixture and heated, at a rate of 10 °C min⁻¹, to a final temperature of 400 °C. Water, which is the only volatile product of the reduction reaction was removed from the exit gas with a cold molecular sieve trap at -17 °C to avoid its interference with the TCD detector.

Catalyst Preparation

Preparation of support. IRMOF-3 was synthesized and activated according to the procedure from literature with slight modifications.^{17,18a} In a typical catalyst preparation, Zn(NO₃)₂·6H₂O (24.900 mmol, 7.480 g) and NH₂-BDC (8.300 mmol, 1.520 g) were dissolved in 200 mL *N,N'*-dimethylformamide (DMF) and stirred for 0.5 h at room temperature in air. The solution was transferred and sealed in a 500 mL Teflon-lined autoclave, and kept at 100 °C for 18 h. The resulting brown solid was collected by centrifugation and washed thrice with DMF and CHCl₃ over three days, and the solid was finally dried in a vacuum at 50 °C.

Dried IRMOF-3 (2.000 g, 2.450 mmol) was dispersed in 15 mL CHCl₃. A solution of salicylaldehyde (1.050 g, 8.600 mmol) in CHCl₃ (15 mL) was dropwise added at room temperature, and stored seven days at room temperature.^{18b} The samples were centrifuged, washed thrice with CHCl₃ and dried in vacuum at 50 °C to yield IRMOF-3-SI.

Preparation of Au catalysts. For the synthesis of Au/IRMOF-3 by post-covalent modification, a solution of NaAuCl₄·2H₂O (0.071 g) in 0.5 mL MeCN was dropwise added to IRMOF-3-SI (0.690 g) at room temperature and was stored overnight. Then the sample was dried in a vacuum at 30 °C for 3 h. The catalyst was denoted as 4.6%Au/IRMOF-3.

The typical procedure for the one-pot synthesis of the Au/IRMOF-3 catalysts: a mixture of NH₂-BDC (0.68 mmol, 0.124 g), salicylaldehyde (0.220 mmol, 0.027 g), and DMF (18 mL) were stirred for 0.5 h at room temperature. Zn(NO₃)₂·6H₂O (2.000 mmol, 0.600 g) was added to the mixture and was stirred for a further 0.5 h. Then a solution of AuCl (0.020 mmol, 0.007 g) in DMF (1 mL) was dropwise added. The mixture was transferred into a Teflon-lined stainless steel vessel and was heated for 24 h at 100 °C. After cooling of the vessel to room temperature, the resulting green solid was collected by centrifugation and was washed thrice with DMF and CHCl₃ over three days. The catalysts were denoted as 0.6%Au/IRMOF-3. 3.2%Au/IRMOF-3 was synthesized using the same molar ratios as for 0.6%Au/IRMOF-3, but using NaAuCl₄·2H₂O (0.020 mmol, 0.015 g) as the Au precursor.

Catalytic measurements. Typical procedure for the A³ coupling reaction: a mixture of catalyst (0.070 g), benzaldehyde (0.250 mmol, 0.027 g), piperidine (0.300 mmol, 0.026 g), phenylacetylene (0.325 mmol, 0.034 g), and 1,4-dioxane (1.000 g) were put into a closed glass reactor (2 mL, SUPELCO) and were extensively stirred (*ca.* 500 rpm) at 120 or 150 °C. After the reaction, the catalyst was removed from the solution by centrifugation at 6000 rpm for 10 minutes. The product was analysed by GC (SP6890, capillary column, SE-30). And the recovered catalyst was thoroughly washed with 1,4-dioxane and used for the next run.

Acknowledgements

We thank the National Natural Science Foundation of China (no. 20903119, 21173269, and 91127040) and Programme for New Century Excellent Talents in University.

References

- (a) A. A. Boulton, B. A. Davis, D. A. Durden, L. E. Dyck, A. V. Juorio, X. M. Li, I. A. Paterson and P. H. Yu, *Drug Dev. Res.*, 1997, **42**, 150; (b) M. Konishi, H. Ohkuma, T. Tsuno, T. Oki, G. D. VanDuynne and J. Clardy, *J. Am. Chem. Soc.*, 1990, **112**, 3715; (c) M. Miura, M. Enna, K. Okuro and M. Nomura, *J. Org. Chem.*, 1995, **60**, 4999; (d) A. Jenmalm, W. Berts, Y. L. Li, K. Luthman, I. Csoeregh and U. Hacksell, *J. Org. Chem.*, 1994, **59**, 1139; (e) G. Dyker, *Angew. Chem., Int. Ed.*, 1999, **38**, 1698.
- (a) R. Bloch, *Chem. Rev.*, 1998, **98**, 1407; (b) M. E. Jung and A. Huang, *Org. Lett.*, 2000, **2**, 2659; (c) T. Murai, Y. Mutoh, Y. Ohta and M. Murakami, *J. Am. Chem. Soc.*, 2004, **126**, 5968.
- (a) C. M. Wei, Z. G. Li and C. J. Li, *Synlett*, 2004, **35**, 1472; (b) F. P. Xiao, Y. L. Chen, Y. Liu and J. B. Wang, *Tetrahedron*, 2008, **64**, 2755.

- 4 C. Wei and C. J. Li, *J. Am. Chem. Soc.*, 2003, **125**, 9584.
- 5 V. K. Y. Lo, Y. Liu, M. K. Wong and C. M. Che, *Org. Lett.*, 2006, **8**, 1529.
- 6 C. Wei, Z. Li and C. J. Li, *Org. Lett.*, 2003, **5**, 4473.
- 7 L. Shi, Y. Q. Tu, M. Wang, F. M. Zhang and C. A. Fan, *Org. Lett.*, 2004, **6**, 1001.
- 8 L. P. Hua and W. Lei, *Chin. J. Chem.*, 2005, **23**, 1076.
- 9 C. J. Li and C. Wei, *Chem. Commun.*, 2002, 268.
- 10 X. Zhang and A. Corma, *Dalton Trans.*, 2008, 397.
- 11 M. Kidwai, V. Bansal, A. Kumar and S. Mozumdar, *Green Chem.*, 2007, **9**, 742.
- 12 K. K. R. Datta, B. V. S. Reddy, K. Ariga and A. Vinu, *Angew. Chem., Int. Ed.*, 2010, **49**, 4971.
- 13 K. Layek, R. Chakravarti, M. L. Kantam, H. Maheswaran and A. Vinu, *Green Chem.*, 2011, **13**, 2878.
- 14 X. Zhang and A. Corma, *Angew. Chem., Int. Ed.*, 2008, **47**, 4358.
- 15 (a) C. Y. Sun, S. X. Liu, D. D. Liang, K. Z. Shao, Y. H. Ren and Z. M. Su, *J. Am. Chem. Soc.*, 2009, **131**, 1883; (b) V. Finsy, L. Ma, L. Alaerts, D. E. D. Vos, G. V. Baron and J. F. M. Denayer, *Microporous Mesoporous Mater.*, 2009, **120**, 221; (c) Y. W. Li and R. T. Yang, *AIChE J.*, 2008, **54**, 269.
- 16 O. M. Yaghi, M. O'Keeffe, N. W. Ockwig, H. K. Chae, M. Eddaoudi and J. Kim, *Nature*, 2003, **423**, 705.
- 17 J. L. C. Rowsell and O. M. Yaghi, *J. Am. Chem. Soc.*, 2006, **128**, 1304.
- 18 (a) K. K. Tanabe, Z. Wang and S. M. Cohen, *J. Am. Chem. Soc.*, 2008, **130**, 8508; (b) X. Zhang, F. X. L. I. Xamena and A. Corma, *J. Catal.*, 2009, **265**, 155; (c) Z. Q. Wang and S. M. Cohen, *J. Am. Chem. Soc.*, 2007, **129**, 12368; (d) S. J. Garibay, Z. Q. Wang, K. K. Tanabe and S. M. Cohen, *Inorg. Chem.*, 2009, **48**, 7341; (e) E. Dugan, Z. Q. Wang, M. Okamura, A. Medina and S. M. Cohen, *Chem. Commun.*, 2008, 3366; (f) M. J. Ingleson, J. P. Barrio, J. B. Guilbaud, Y. Z. Khimyak and M. J. Rosseinsky, *Chem. Commun.*, 2008, 2680.
- 19 (a) M. Eddaoudi, J. Kim, N. Rosi, D. Vodak, J. Wachter, M. O'Keeffe and O. M. Yaghi, *Science*, 2002, **295**, 469; (b) J. Gascon, U. Aktay, M. D. Hernandez-Alonso, G. P. M. Klink and F. Kapteijn, *J. Catal.*, 2009, **261**, 75.
- 20 L. M. Huang, H. T. Wang, J. X. Chen, Z. B. Wang, J. Y. Sun, D. Y. Zhao and Y. S. Yan, *Microporous Mesoporous Mater.*, 2003, **58**, 105.
- 21 (a) Y. W. Li and R. T. Yang, *Langmuir*, 2007, **23**, 12937; (b) J. G. Nguyen and S. M. Cohen, *J. Am. Chem. Soc.*, 2010, **132**, 4560; (c) N. R. Stuckert, L. F. Wang and R. T. Yang, *Langmuir*, 2010, **26**, 11963.
- 22 S. J. Wang, X. X. He, L. X. Song and Z. Y. Wang, *Synlett*, 2009, 447.
- 23 S. J. Garibay, Z. Q. Wang and S. M. Cohen, *Inorg. Chem.*, 2010, **49**, 8086.
- 24 J. H. He, Y. T. Zhang, J. H. Yu, Q. H. Pan and R. R. Xu, *Mater. Res. Bull.*, 2006, **41**, 925.
- 25 (a) G. J. Hutchings, M. S. Hall, A. F. Carley, P. Landon, B. E. Solsona, C. J. Kiely, A. Herzing, M. Makkee, J. A. Moulijn, A. Overweg, J. C. Fierro-Gonzalez, J. Guzman and B. C. Gates, *J. Catal.*, 2006, **242**, 71; (b) N. A. Hodge, C. J. Kiely, R. Whyman, M. R. H. Siddiqui, G. J. Hutchings, Q. A. Pankhurst, F. E. Wagner, R. R. Rajaram and S. E. Golunski, *Catal. Today*, 2002, **72**, 133; (c) X. Zhang, H. Shi and B. Q. Xu, *J. Catal.*, 2011, **279**, 75.
- 26 (a) Z. Q. Wang, K. K. Tanabe and S. M. Cohen, *Inorg. Chem.*, 2009, **48**, 296; (b) Q. L. Li, Y. H. Zhang, G. X. Chen, J. Q. Fan, H. Q. Lan and Y. Q. Yang, *J. Catal.*, 2010, **273**, 167.
- 27 X. Zhang and A. Corma, *Chem. Commun.*, 2007, 3080.
- 28 (a) K. M. Reddy, N. S. Babu, I. Suryanarayana, P. S. S. Prasad and N. Lingaiah, *Tetrahedron Lett.*, 2006, **47**, 7563; (b) H. Z. S. Huma, R. Halder, S. S. Karla, J. Das and J. Iqbal, *Tetrahedron Lett.*, 2002, **43**, 6485.
- 29 B. Huang, X. Yao and C. J. Li, *Adv. Synth. Catal.*, 2006, **348**, 1528.
- 30 M. L. Kantam, B. V. Prakash, C. R. V. Reddy and B. Sreedhar, *Synlett*, 2005, 2329.